THE JOURNAL OF PHYSICAL CHEMISTRY Letters

Letter

pubs.acs.org/JPCL

Hybrid Titania Photoanodes with a Nanostructured Multi-Layer Configuration for Highly Efficient Dye-Sensitized Solar Cells

Hui-Ping Wu,[†] Chi-Ming Lan,[†] Jyun-Yu Hu,[†] Wei-Kai Huang,[†] Jia-Wei Shiu,[†] Zih-Jian Lan,[†] Cheng-Ming Tsai,[†] Chun-Hsien Su,[‡] and Eric Wei-Guang Diau*[,†]

[†]Department of Applied Chemistry and Institute of Molecular Science, National Chiao Tung University, No.1001, Ta Hsueh Road, Hsinchu 30010, Taiwan

[‡]Mechanical and Systems Research Laboratories, Industrial Technology Research Institute (ITRI), 195, Section 4, Chung Hsing Road, Hsinchu 31040, Taiwan

Supporting Information

ABSTRACT: To construct a hybrid titania photoanode containing nanoparticles and nanorods of varied size in a multilayer (ML) configuration for dye-sensitized solar cells, the essence of our ML design is a bilayer system with additional layers of nanorods of well-controlled size inserted between the transparent and the scattering layers to enhance the light-harvesting capability for photosensitizers with small absorptivity, such as Z907. We measured charge-extraction and intensity-modulated photoelectric spectra to show the advantages of one-dimensional nanorods with an improved electron-transport property and an upward shift of the potential band edge; a favorable ML configuration was constructed to have a cascade potential feature for feasible electron transport from long nanorods, to normal nanorods, to small nanoparticles. On the basis of the ML system reported herein, we demonstrate how the performance of a Z907 device is improved to attain η ~10%, which is a milestone for its future commercialization.

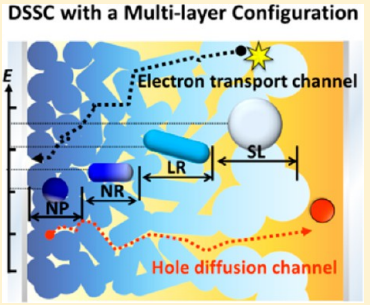

SECTION: Energy Conversion and Storage; Energy and Charge Transport

Nanostructured TiO_2 has many applications in photocatalysis, sensors, batteries, memory resistors, water splitting, solar cells, and so forth.[1−3] Among these applications, TiO_2 has been widely utilized as an efficient mediator to transport electrons in the working electrode of a dye-sensitized solar cell (DSSC).[4−7] For a typical DSSC, a TiO_2 film is designed with a bilayer structure: a scattering layer (SL) of thickness 2−5 μm on top of a transparent TiO_2 active layer (AL) of thickness 12−14 μm;[8−11] for an AL, anatase TiO_2 nanoparticles (NPs) of size ~20 nm were employed to attain sufficient proportions of dye-loading (DL) for light harvesting in the visible spectral region;[8,9] for a SL, particles of size 200−400 nm were introduced to enhance the light harvesting at wavelengths 600−800 nm.[10−12] To provide direct channels for electron transport in DSSC, various one-dimensional (1D) TiO_2 nanostructures, such as nanotube arrays,[13,14] nanowire arrays,[15,16] nanofibers[17,18] and nanorods of varied sizes,[19−26] were developed. These 1D TiO_2 nanostructures benefit from improved efficiencies of charge collection, but the surface areas smaller than their NP-based counterparts limit the DL on the TiO_2 surface to further promote the device performance. Numerous efforts are reported to enhance the DL for 1D TiO_2 photoanodes: one approach is to combine the 1D nanostructures with conventional NP in a blend composite;[27−31] a second approach is to form a bifunctional 1D hierarchical structure,[32−36] which is similar to the design of a spherical bead with a 3D hierarchical morphology;[12,37−39] a third approach is to make a double-layered film structure similar to a conventional NP-based device, but with the AL and SL replaced by small and large 1D TiO_2 nanostructures, respectively.[36,40]

In general, four major factors to consider in the development of a high-performance TiO_2 photoanode are (1) a large specific surface area for sufficient DL, (2) an excellent scattering effect for enhanced light harvesting, (3) a superior electron-transport characteristic for efficient charge collection, and (4) adequate porosity of the film for feasible diffusion of the electrolyte. These key factors are, however, generally mutually incompatible, so that these sophisticated approaches fail to attain efficiencies comparable with or superior to that of a conventional NP-based device.[41,42] For example, it is difficult to simultaneously increase the surface area and light scattering in one monolayer of TiO_2, whereby flexibility results from a bilayered structure to separate the AL and the SL on the TiO_2 film. Use of TiO_2 NP of size ~20 nm as an AL in a bilayered system confers an advantage of a large surface area, but the thickness of the film cannot exceed ~15 μm because the existence of many grain boundaries in NP limits the efficient electron transport.[9] One remedy for this problem is to incorporate promising 1D nanostructures as other layers to enhance the DL for improved light-harvesting efficiency, but at the same time to retain the excellent 1D electron-transport

Received: March 20, 2013
Accepted: April 19, 2013

   dx.doi.org/10.1021/jz400620q | J. Phys. Chem. Lett. 2013, 4, 1570−1577

feature in the film for improved efficiency of charge collection. We therefore constructed a hybrid TiO_2 film with a multilayer (ML) morphology[43] to accommodate all incompatible key factors required to make a highly efficient DSSC.

Figure 1 demonstrates the concept for the structural design of a hybrid titania ML film. The basic idea is to maintain the original effective design of the bilayer system with conventional small TiO_2 NPs and large SLs, but we added 1D TiO_2 nanorods of varied size between the NP and SL layers to form a hybrid TiO_2 film with the ML configuration shown in Figure 1, left. The additional 1D titania layers should have a function to further enhance the specific surface area and the effect of light scattering with nanorods of small and large sizes, respectively. Moreover, each layer in the film must be arranged to have a size in a systematic sequence so that the porosity of the film can be readily tuned to produce a suitable mesoporous network environment for diffusion of the electrolyte. According to this approach to construct the ML film, we thus designed TiO_2 nanorods of three types, labeled SR, NR, and LR with lengths ~40, ~150, and ~500 nm, respectively. Figure 1 right shows a side-view scanning electron microscopy (SEM) image of a typical ML film of thickness ~26 μm.

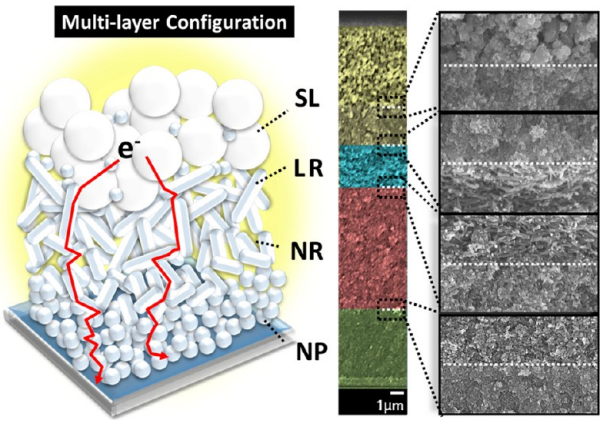

Figure 1. Schematic demonstration of the concept for the structural design of a hybrid TiO_2 ML film.

The synthesis of TiO_2 nanorods of normal size (NR) involved a simple hydrothermal method[20] using titanium tetraisopropoxide (TTIP) as a precursor in a basic aqueous solution containing (1) diaminoethane (DAE) as a catalyst for crystal growth, and (2) triblock copolymer PEO_{106}–PPO_{70}–PEO_{106} (F127) and cetyltrimethylammonium bromide (CTAB) as functional surfactants to control the anisotropic growth of the 1D nanostructure. For the growth of short nanorods (SR), oleic acid (OA) was added at a small fraction to the aqueous solution containing the same TTIP/ethylenediamine (EDA)/CTAB/F127 mixture. To produce the long nanorods (LRs), much triethanolamine (TEOA) was added to the same aqueous solution to retard the hydrolysis, with both the peptization and hydrothermal periods being twice those of the growth of NRs and SRs. Top-view SEM images of SRs, NRs, and LRs appear in Figure 2a–c, respectively. Figures 2d–f shows transmission electron microscopy (TEM) images for SR, NR, and LR, respectively; Figure 2g–i shows the correspondingly magnified TEM images, indicating the distance between adjacent (101) lattice fringes of anatase TiO_2 to be 0.35 nm. The formation of purely crystalline nanostructures in the anatase phase for the NP, SR, NR, and LR species was

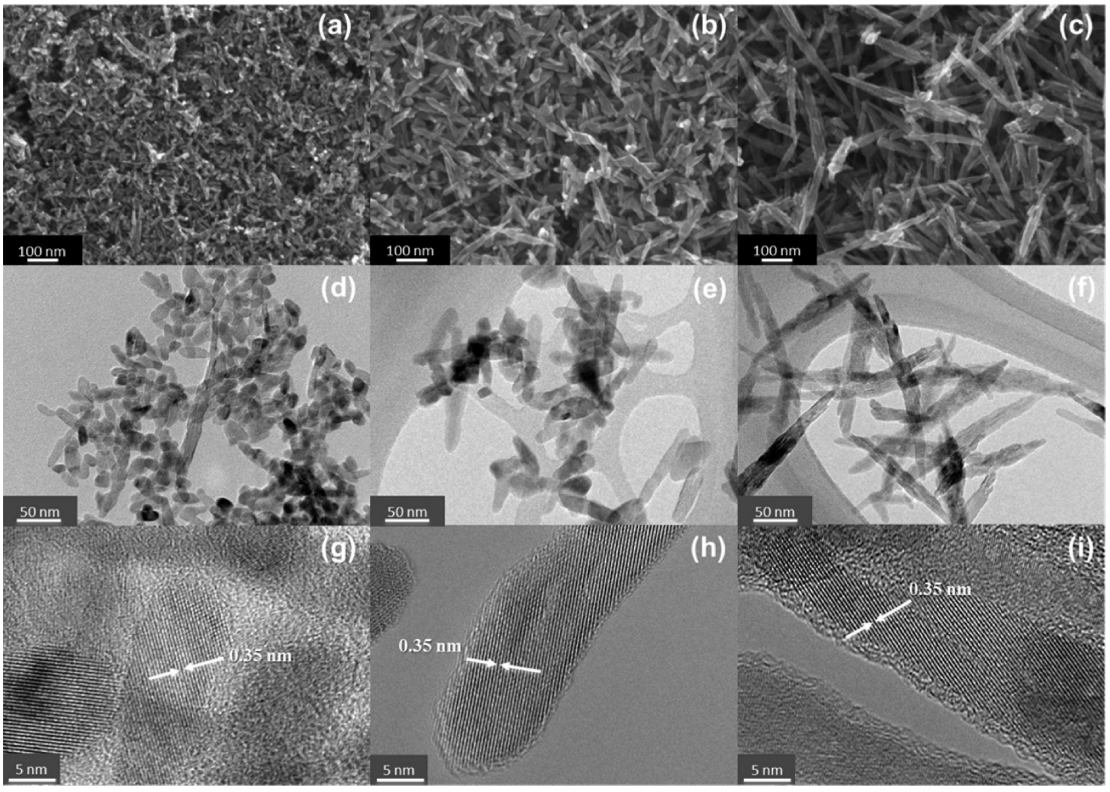

Figure 2. SEM images of (a) SR, (b) NR, and (c) LR; TEM images of (d) SR, (e) NR, and (f) LR. (g–i) HRTEM images of SR, NR, and LR, respectively. The arrows shown in panels g–i mark the specific distance of the adjacent lattice fringes along the (101) facet of anatase TiO_2.

dx.doi.org/10.1021/jz400620q | J. Phys. Chem. Lett. 2013, 4, 1570–1577

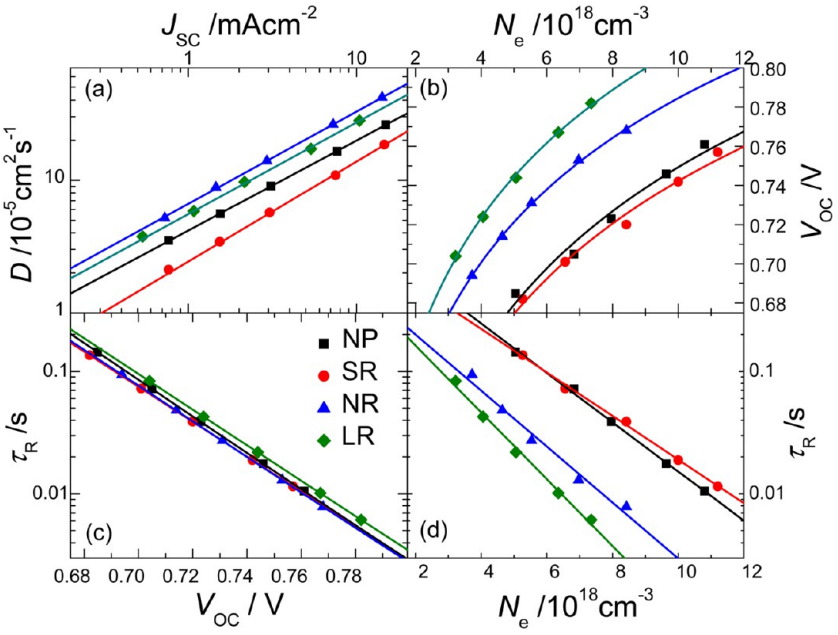

Figure 3. Characteristic plots of (a) electron diffusion coefficient (D) vs J_{SC}, (b) V_{OC} vs charge density (N_e), (c) electron lifetime (τ_R) vs V, and (d) τ_R vs N_e for devices containing only a single layer (NP, SR, NR or LR) of thickness ~11 μm.

confirmed with X-ray diffraction (XRD) patterns shown in Figure S1, Supporting Information.

To examine the intrinsic photovoltaic properties of each 1D nanostructure, we fabricated DSSC devices according to the experimental procedure as reported elsewhere,[9] but with the photoanodes constructed of NP, SR, NR, or LR in a single layer; the thickness of each nanostructure was carefully controlled to be ~11 μm. Amphiphilic dye Z907 served as a standard photosensitizer for our tests because of its superior endurance.[44] The current−voltage (J−V) characteristics of these devices are shown in Figure S2a, and the corresponding IPCE action spectra in S2b; the photovoltaic parameters are summarized in Table S1. We found a systematic trend for the short-circuit current densities (J_{SC}) with NP ~SR > NR > LR, but the trend for the open-circuit voltages (V_{OC}) is reversed, LR > NR > SR ~NP. The trend of J_{SC} is consistent with that of DL (Table S1), and the poor performance, η = 5.8%, of the LR device resulted from its smaller surface area giving a smaller DL. In contrast, as J_{SC} and V_{OC} were complementary to each other for the NP, SR, and NR, these devices attained similar efficiencies of power conversion in the range η = 7.3−7.5%. To understand the electron-transport characteristics of the four devices, we accordingly measured intensity-modulated photocurrent spectra (IMPS), intensity-modulated photovoltage spectra (IMVS), and charge extraction (CE);[6] the results appear in Figure 3.

Figure 3a shows plots of diffusion coefficient D versus J_{SC} obtained from IMPS measurements; the results indicate a trend of electron diffusion on TiO_2 with order NR > LR > NP > SR when they were compared at the same J_{SC} level. That the electron diffusion of LR is less than that of NR might be understood from the morphological features of the nanostructures, for which the formation of LR involved an aggregation of a few sub-LR units unambiguously seen in the TEM image, Figure 2f. The poor diffusion of SR, also unexpected, might be due to the effect of OA bound on the TiO_2 surface that was difficult to remove completely via postannealing. NR has thus the best diffusion characteristic among all TiO_2 nanostructures under investigation. Figure 3b shows the CE results under an open-circuit condition, giving a systematic trend for the TiO_2 potential shifts of the conduction band edge with order LR > NR > NP > SR; relative to that of NP, the potentials of LR and NR were increased, whereas that of SR was decreased. The positions of the TiO_2 potentials compared at the same electron densities (N_e) are consistent with the variation of V_{OC} in Table S1. Figure 3c shows plots of electron lifetime (τ_R) versus V_{OC} at the open-circuit condition. All devices had fortuitously similar τ_R values, but the longer nanorod LR exhibited electron lifetimes slightly greater than the others when they were compared at the same V_{OC} level. This result seems consistent with many other studies that show retarded charge recombination for electron lifetimes of 1D nanostructures smaller than those of NP compared at the same V_{OC} level,[17] at the same J_{SC} level,[21,24,30] or at the same level of bias light intensity.[29,32,40] When the electron lifetimes were compared at the same N_e level, the trend was SR ~NP > NR > LR shown in Figure 3d: this result is consistent with a conclusion reported after comparison of the electron-transport properties between NP-based and nanowire-based solar cells.[16] Longer nanorods (LR and NR) with a superior electron-diffusion characteristic (Figure 3a) and greater potentials (Figure 3b) also displayed more rapid recombination of charge (Figure 3d) than NP and SR, but our results indicate that the magnitudes of V_{OC} were controlled mainly by the positions of the TiO_2 potentials; the retarded charge recombination played only a minor role.

According to the superior electron transport and increased potential of NR, we selected NR as part of the AL in our ML system. To examine the combined effects of NP and NR, we constructed TiO_2 photoanodes with a bilayer structure containing NP and NR components as bottom and top layers, respectively, in varied ratios, labeled NP5, NP4/NR1, NP3/NR2, NP2/NR3, NP1/NR4, and NR5, in which the numbers represent the repeated screen-printing times of each component. The thicknesses of the films increased gradually from 10.6 μm of NP to 13.5 μm of NR, and DL/nmol cm^{-2} also decreased accordingly from 122 of NP to 108 of NR

dx.doi.org/10.1021/jz400620q | J. Phys. Chem. Lett. 2013, 4, 1570−1577

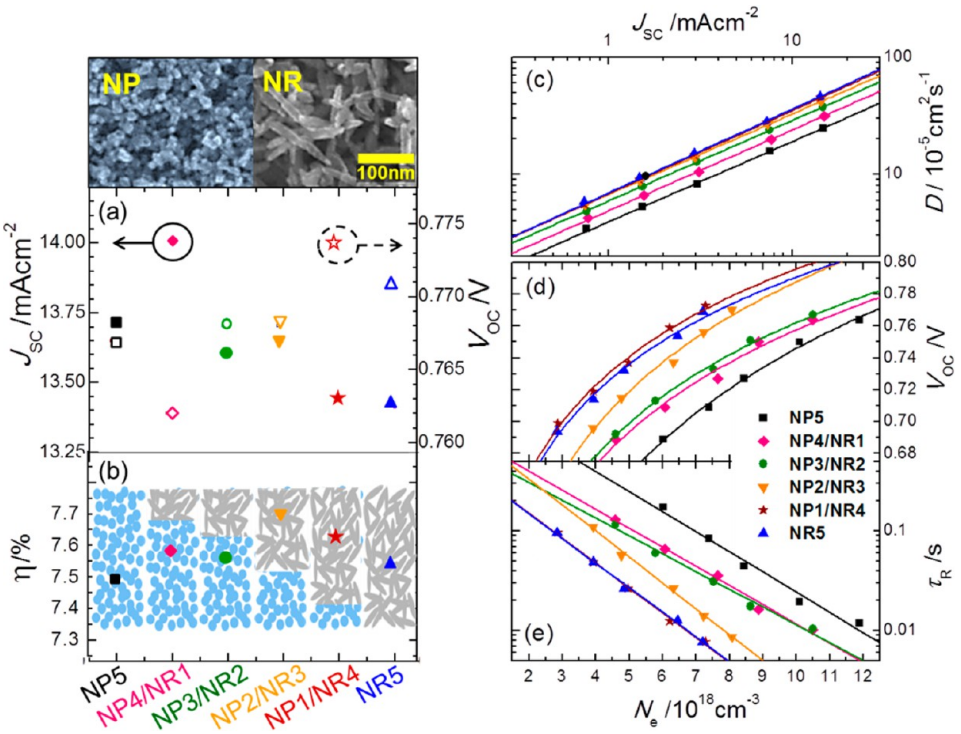

Figure 4. Photovoltaic performance of double-layer devices containing NP and NR components in varied ratios: (a) short-circuit current density (J_{SC}, filled symbols) and open-circuit voltage (V_{OC}, open symbols); (b) efficiency η of power conversion; (c) electron diffusion coefficient (D) vs J_{SC}; (d) V_{OC} vs charge density (N_e); (e) electron lifetime (τ_R) vs N_e. SEM images of NP and NR at the top left side have the film compositions of each device structurally represented inside panel b.

(Table S2). Figure S3a displays the *JV* curves and Figure S3b the corresponding IPCE action spectra of these devices; the photovoltaic parameters are summarized in Table S2. Figure 4a,b exhibits a systematic trend of photovoltaic performance of this series: J_{SC} decreases, whereas V_{OC} increases upon increasing the contribution of NR. Because the variations of both J_{SC} and V_{OC} opposed each other, the efficiencies of power conversion of the bilayer system varied only slightly within a range η = 7.5−7.7%; the maximum efficiency occurred at the NP2/NR3 composition.

Figure 4c shows plots of D vs J_{SC} obtained from the IMPS measurements. These results confirm the superior electron transport of NR and show almost identical diffusion characteristics for the configurations varied from NR5 to NP2/NR3; this electron transport begins to decrease from NP3/NR2 to NP5. Judging from the CE and IMVS results shown in Figure 4d,e, we confirm the systematic variations on increasing the TiO_2 potentials and accelerating the rates of charge recombination with increased contribution of NR in this bilayer system. On the basis of both photovoltaic and electron-transport properties demonstrated in Figure 4, we understand that a thin layer of NP is necessary for two reasons: to retain sufficient DL for enhanced J_{SC}, and to retard the charge recombination at the bottom layer of the ML configuration. An idea for a design of an optimal ML configuration for DSSC is thus achievable based on the NP/NR bilayer system with additional LR and SL layers to significantly enhance the effect of light scattering to improve J_{SC}.

The effect of the SL to enhance J_{SC} is expected to be significant. In our approach, the SL contains mixed TiO_2 NPs in two layers of varied size. The first SL layer (SL-1, thickness ∼3 μm) contains the commercially available ST41 (particle size 200−400 nm) mixed with NP in mass ratio ST41/NP = 50/50, whereas the second SL layer (SL-2, thickness ∼6 μm) contains the ST41/NP mixture at mass ratio 80/20. Figures S4a and S4b show top-view SEM images of the SL-1 and SL-2 layers, respectively. The design to involve small NP in the SL has two purposes: to increase the DL, and to improve the connectivity of the large NPs for a robust structure. As a result, J_{SC} increased ∼30% when the bilayered SL-1/SL-2 film of thickness ∼9 μm was added on top of the bilayered NP2/NR3 film of thickness ∼13 μm, yielding an overall cell performance (device **C**; Table 1) η = 9.5%. The ML system was hence designed with NP and SL of fixed thicknesses ∼5 μm and ∼9 μm, respectively, but with those of NR and LR systematically varied according to a ML configuration, NP/NR/LR/SL-1/SL-2; the number of each layer represents the repeated times of screen printing of each component. Figure 5a−c presents side-view SEM images, *JV* characteristic curves, and IPCE action spectra of these devices, labeled **A**−**F**, respectively. Table 1 summarizes the photovoltaic parameters of these ML devices and the corresponding shun resistances (R_{sh}) determined from the *JV* curves.

As indicated in the SEM images shown in Figure 5a, devices **A**−**D** were designed to assess the effect of the NR layer (shown as red foreground) on the photovoltaic performance under constant contributions of the NP (green foreground), SL-1 and SL-2 layers; the thicknesses of the NR layer were controlled to be 3.0, 6.2, 8.7, and 10.9 μm for devices **A**−**D**, respectively. Devices **E** and **F** were designed to assess the effect of the LR layer (blue foreground) on the photovoltaic performance based on the structure of device **C**. First, according to the photovoltaic results in Figure 5b,c, we observed a systematically increasing trend of J_{SC} upon increasing the contributions of NR from device **A** to device **D**, leading to the performance of device **D** attaining J_{SC} = 18.58 mA cm^{-2} and η = 9.66%. The decreases of V_{OC} and FF upon increasing the film thickness from device **A**

dx.doi.org/10.1021/jz400620q | *J. Phys. Chem. Lett.* 2013, 4, 1570−1577

Table 1. Total Thickness (L) of Titania Film and Photovoltaic Parameters of Devices Made of Z907 Dye, and ML TiO_2 Films with Varied Film Configurations Defined as A–F under Simulated AM-1.5G Illumination (Power Density 100 mW cm^{-2}) and Active Area 0.16 cm^2 with a Black Mask of Area of 0.25 cm^2

device	TiO_2 film configuration[a]	L/ μm	J_{SC}/ mA cm^{-2}	V_{OC}/ mV	FF	η/%	R_{sh}/ kΩ
A	2/**1**/0/1/2	17	15.82	774	0.731	8.95	12.7
B	2/**2**/0/1/2	20	16.74	772	0.727	9.39	12.0
C	2/**3**/0/1/2	22	17.49	761	0.713	9.49	11.5
D	2/**4**/0/1/2	25	18.58	749	0.694	9.66	10.9
E	2/**3**/**1**/1/2	26	18.29	755	0.709	9.79	11.1
F	2/**3**/**2**/1/2	30	18.15	749	0.709	9.64	11.1

[a]The ML films have a typical layer configuration NP/NR/LR/SL-1/SL-2 with the number of each layer representing the repeated screen-printing times, which were fixed at 2, 1, and 2 for the layers of NP, SL-1, and SL-2, respectively. The film thicknesses/μm of the NP, SL-1 and SL-2 layers are in the ranges 4.5–4.9, 2.8–3.2, and 6.0–6.3, respectively. The film thicknesses/μm of the NR layer are 3.0, 6.2, 8.7, 10.9, 9.1, and 8.8 for devices **A**–**F**, respectively, whereas those of the LR layer are 2.9 and 6.3 for devices **E** and **F**, respectively.

to device **D** can be understood from the variation of R_{sh} (Table 1) showing a systematic decreasing trend. Second, with device **C** as a reference, devices **E** and **F** were constructed with additional LR layers of thicknesses 2.9 and 6.3 μm, respectively. For device **E** with configuration 2/3/1/1/2, the enhancement of J_{SC} was less than for device **D**, but both V_{OC} and FF had a balance better than that of device **D** to attain a superior performance of device **E**. This is also reflected by the results of R_{sh} (Table 1) showing a slight increase on shun resistance from device **D** to device **E** due to the contribution of LR. Further increasing the contribution of LR in device **F** caused a slight degradation of all three photovoltaic parameters relative to those of device **E**. The best cell performance of Z907 occurred for device **E** with these characteristics: J_{SC}/mA cm^{-2} = 18.29, V_{OC}/mV = 755, FF = 0.709, and η = 9.79%.

This hybrid ML photoanode system has a flexibility to adjust the contribution of each layer so that this approach becomes versatile for use in photosensitizers of other types. For example, we also examined a thiophene-based heteroleptic Ru complex (C106)[46] with large absorptivity in our ML system to perform best at the device **C** configuration; work is in progress to examine other prospective dyes with this ML approach. The device performances of Z907 and C106 have been further optimized at film configurations **E** and **C**, respectively, treated with an antireflection coating on the surface of the fluorine-doped tin oxide (FTO) substrate opposite the TiO_2 film. Figures S5a and S5b present optimized JV curves and the corresponding IPCE action spectra of devices Z907 and C106, respectively; the photovoltaic performances of both sensitizers optimized with conventional TiO_2 films of a double-layer configuration, NP at 10 μm and SL-2 at 6 μm, are indicated also as dashed curves. For Z907, optimized device **E** featured J_{SC}/ mA cm^{-2} = 18.59, V_{OC}/mV = 751, FF = 0.710 and η = 9.91%;

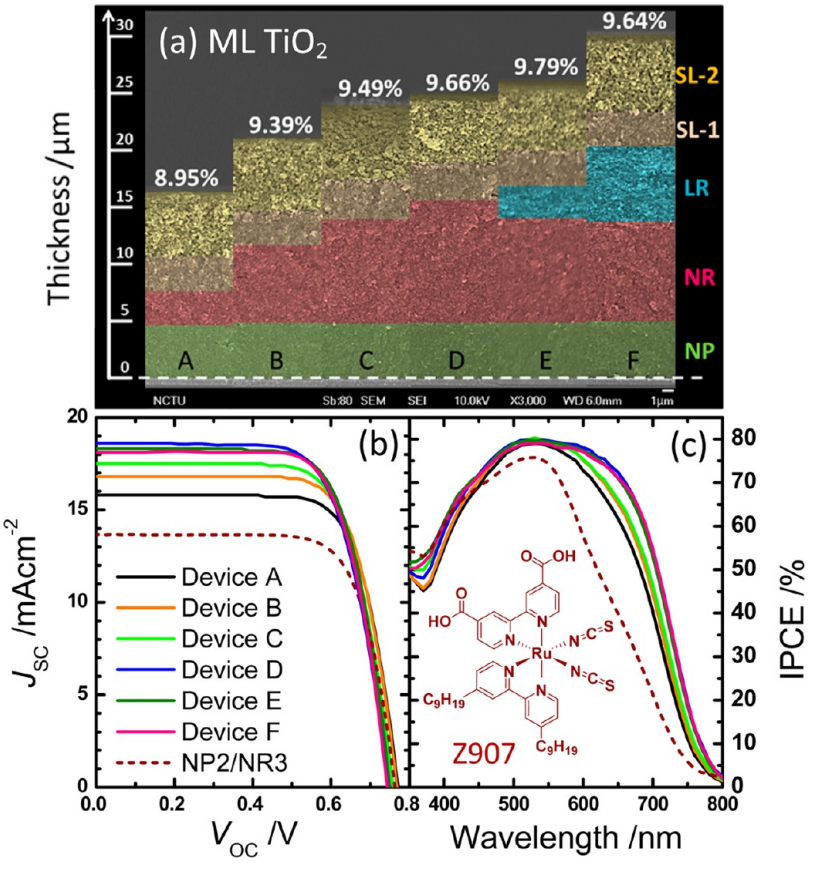

Figure 5. (a) Side-view SEM images of TiO_2 films showing ML configurations for devices **A**–**F**; (b) JV characteristic curves and (c) IPCE action spectra of devices **A**–**F** (solid curves in distinct colors) and the reference bilayer device NP2/NR3 (dashed curve) sensitized with Z907 dye. The molecular structure of Z907 is indicated inside panel c.

dx.doi.org/10.1021/jz400620q | J. Phys. Chem. Lett. 2013, 4, 1570–1577

for C106, the optimized device **C** exhibited J_{SC}/mA cm^{-2} = 19.04, V_{OC}/mV = 754, FF = 0.732, and η = 10.51%; both devices are significantly superior to their NP-based bilayer counterparts (9.3% and 9.8% for Z907 and C106, respectively), giving a promising perspective to promote the device performance for a DSSC based on our ML approach.

The heteroleptic ruthenium complex, Z907, exhibits outstanding performance stability under enduring thermal stress and light-soaking conditions to match the industrial standard of silicon solar cells for outdoor applications;[45] the device performance was first reported to be only η = 7.8% because of the small absorption coefficients of Z907,[44] then improved to η = 9.1% based on a bilayer film system of high quality.[46,47] With our ML system reported here, we demonstrate for the first time how the performance of a Z907 device becomes improved to attain η ∼10%, which is a milestone for a future DSSC to be commercialized.

In summary, we developed 1D titania nanorods of varied lengths—SRs, NRs, and LRs—to serve as dye-uptake and electron-transport media for DSSCs. These nanostructures were synthesized with a simple hydrothermal method using TTIP as a precursor in a basic aqueous solution containing F127 and CTAB; the sizes of the nanorods were controlled on adding OA and TEOA, respectively. CE, IMPS and IMVS were measured to understand the shifts of the TiO_2 conduction band edges, electron diffusion and kinetics of charge recombination in devices made of these nanorods. We discovered a systematic variation of increased potential with order LR > NR > NP > SR; this property is consistent with the variation of V_{OC} that is inexplicable according to the extent of charge recombination. Both NR and LR feature electron transport better than that of NP; they become suitable candidates to construct a hybrid titania photoanode for DSSC with a ML configuration in addition to the conventional NP/SL bilayer system. The designed ML configuration has structure NP/NR/LR/SL for two reasons. First, the particle sizes increase gradually from the bottom layer (NP) to the top layer (SL), so that a suitable mesoporous network becomes available for electrolyte diffusion. Second, the order of potential positions of these nanostructures is correct so that an appropriate sequence of energy cascade becomes established for feasible electron transport from SL (ST41 mixed with a portion of NP), LR, NR to NP. A strategy with hybrid ML photoanodes to attain a great device performance has been achieved for an amphiphilic sensitizer, Z907, which exhibits excellent thermal stability but suffers from its small absorptivity. The Z907 device has been optimized based on the ML system with a typical NP/NR/LR/SL-1/SL-2 configuration to attain η ∼ 10%, which is a promising advance for its future commercialization.

METHODS

Preparation of TiO_2 Nanorods. The NRs, SRs, and LRs were synthesized according to a standard procedure reported elsewhere,[20] but we modified the recipe to control the size of the nanorods in a systematic manner; details follow. First, block copolymer PEO_{106}-PPO_{70}-PEO_{106} (3.0 g, F127, Aldrich) was dissolved in deionized (DI) water (100 mL) and stirred for 15 min at 35 °C. Second, CTAB (1.82 g, 99+%, Aldrich) was added to the flask containing the F127 aqueous solution and stirred for another 15 min at 35 °C. Third, DAE (1.34 mL, 99+ %, Aldrich) was added to the flask containing the mixed F127/CTAB aqueous solution and stirred for 5 min at 35 °C. At this stage, the prepared F127/CTAB/EDA aqueous solution served as a common mediator for preparation of all three nanorods before the peptization and hydrothermal treatments. For NR, TTIP (6.5 mL, 97%, Aldrich) was slowly added to the F127/CTAB/EDA aqueous solution and then stirred for 12 h at 35 °C. For SR, TTIP (6.5 mL) was added slowly to a beaker containing OA (1.9 mL, 95+ %, Showa) for 5 min at 25 °C; the TTIP/OA mixture turned pale yellow, which indicated the formation of an OA-chelated titanium complex. Then the TTIP/OA mixture was added slowly to the F127/CTAB/EDA aqueous solution and stirred for 12 h at 35 °C. After peptization, the white solution was transferred into an autoclave (Teflon) and heated to 160 °C for 12 h to complete the hydrothermal process for both NR and SR.

For LR, TTIP (6.5 mL) was added slowly to a beaker containing TEOA (7.2 mL, 95+ %, TEDIA) and stirred for 5 min at 25 °C; the TTIP/TEOA mixture turned pale yellow, which indicated the formation of a TEOA−chelated titanium complex. The TTIP/TEOA mixture was added slowly to the F127/CTAB/EDA aqueous solution and then stirred for 24 h at 35 °C. After peptization, the white gel-type solution was transferred into an autoclave (Teflon) and heated to 160 °C for 24 h to complete the hydrothermal process. These TiO_2 nanorods were then collected on centrifugation, and washed several times with ethanol. Eventually, to prepare a screen-printable paste for all NPs and nanorods, ethyl cellulose and α-terpineol were added to the ethanol solution of the TiO_2 nanostructures; ethanol was then removed from the solution with a rotary evaporator to obtain a viscous paste suitable for screen printing according to a procedure reported elsewhere.[48] The details to characterize the film morphology are given elsewhere.[9]

Fabrication of DSSC. The DSSC devices were fabricated with a working electrode based on hybrid nanostructured ML TiO_2 films and a Pt-coated counter electrode. For the working electrode, according to the ML configuration for each layer, the target TiO_2 paste (NP, NR, SR, LR, SL-1 or SL-2) was coated on a $TiCl_4$-treated FTO glass substrate (TEC 7, Hartford, USA) to obtain a film of the required thickness (active size 0.4 × 0.4 cm^2) with repetitive screen printing. The TiO_2 film was annealed according to a programmed procedure, followed by a $TiCl_4$ post-treatment reported previously.[9,11] For the dye uptake, the TiO_2 film was immersed in a solution containing either Z907 and CDCA or C106 and CDCA (all 0.3 mM) in a mixture of acetonitrile and *t*-butanol (v/v = 1: 1) kept at 25 °C for 3 h (Z907) or 2 h (C106). For the counter electrode, a solution containing platinum (H_2PtCl_6 in isopropanol) was spin-coated onto the FTO glass at 2000 rpm for 10 s; the electrode as deposited was heated at 380 °C for 30 min.The dye-sensitized working electrode was assembled with the Pt-coated counter electrode into a cell of sandwich type and sealed with a hot-melt film (SX1170, thickness 60 μm) under thermal compression at 90 °C for 10 s. The electrolyte injected into the device contains GuNCS (0.1 M), I_2 (0.03 M), LiI (0.05 M), PMII (1.0 M), 4-*t*-butylpyridine (0.5 M) in acetonitrile, the same for both Z907 and C106. The details of photovoltaic measurements are reported elsewhere.[9,11]

Impedance Characterization. The IMPS and IMVS spectra were measured with CIMPS instruments (Zahner) at a short-circuit or an open-circuit condition, respectively, based on white LED light at five intensities (1.5−30 mW cm^{-2}) controlled with a slave system (XPOT, Zahner) to obtain the photovoltaic response induced by the modulated light.[6] The modulated light was driven with a perturbation current (10%

dx.doi.org/10.1021/jz400620q | J. Phys. Chem. Lett. 2013, 4, 1570−1577

ac) superimposed on a dc current in the frequency range 0.1−1000 Hz. The measurements of CE were performed with the same CIMPS system under the same bias light irradiations; details are given elsewhere.[6]

■ ASSOCIATED CONTENT

Supporting Information

Figures S1−S5 and Tables S1−S2. This material is available free of charge via the Internet at http://pubs.acs.org.

■ AUTHOR INFORMATION

Corresponding Author

*E-mail: diau@mail.nctu.edu.tw.

Notes

The authors declare no competing financial interest.

■ ACKNOWLEDGMENTS

We thank Everlight Chemical Industrial Corporation, Taiwan, for providing Z907 and C106 dyes. The National Science Council of Taiwan and Ministry of Education of Taiwan, under the ATU program, provided financial support of this project.

■ REFERENCES

(1) Chen, X.; Mao, S. S. Titanium Dioxide Nanomaterials: Synthesis, Properties, Modifications, and Applications. *Chem. Rev.* **2007**, *107*, 2891−2959.

(2) Szot, K.; Rogala, M.; Speier, W.; Klusek, Z.; Besmehn, A.; Waser, R. TiO_2 − A Prototypical Memristive Material. *Nanotechnology* **2011**, *22*, 254001.

(3) Khataee, A.; Mansoori, G. A. *Nanostructured Titanium Dioxide Materials: Properties, Preparation and Applications*; World Scientific: Singapore, 2012.

(4) Hagfeldt, A.; Boschloo, G.; Sun, L.; Kloo, L.; Pettersson, H. Dye-Sensitized Solar Cells. *Chem. Rev.* **2010**, *110*, 6595−6663.

(5) Tétreault, N.; Grätzel, M. Novel Nanostructures for Next Generation Dye-Sensitized Solar Cells. *Energy Environ. Sci.* **2012**, *5*, 8506−8516.

(6) Li, L.-L.; Chang, Y.-C.; Wu, H.-P.; Diau, E. W.-G. Characterisation of Electron Transport and Charge Recombination Using Temporally Resolved and Frequency-Domain Techniques for Dye-Sensitised Solar Cells. *Int. Rev. Phys. Chem.* **2012**, *31*, 420−467.

(7) Li, L.-L.; Diau, E. W.-G. Porphyrin-Sensitized Solar Cells. *Chem. Soc. Rev.* **2013**, *42*, 291−304.

(8) Ito, S.; Murakami, T. N.; Comte, P.; Liska, P.; Grätzel, C.; Nazeeruddin, M. K.; Grätzel, M. Fabrication of Thin Film Dye Sensitized Solar Cells with Solar to Electric Power Conversion Efficiency over 10%. *Thin Solid Films* **2008**, *516*, 4613−4619.

(9) Shiu, J.-W.; Lan, C.-M.; Chang, Y.-C.; Wu, H.-P.; Huang, W.-K.; Diau, E. W.-G. Size-Controlled Anatase Titania Single Crystals with Octahedron-Like Morphology for Dye-Sensitized Solar Cells. *ACS Nano* **2012**, *6*, 10862−10873.

(10) Koo, H. J.; Park, J.; Yoo, B.; Yoo, K.; Kim, K.; Park, N. G. Size-Dependent Scattering Efficiency in Dye-Sensitized Solar Cell. *Inorg. Chim. Acta* **2008**, *361*, 677−683.

(11) Lan, C.-M.; Liu, S.-E.; Shiu, J.-W.; Hu, J.-Y.; Lin, M.-H.; Diau, E. W.-G. Formation of Size-Tunable Dandelion-like Hierarchical Rutile Titania Nanospheres for Dye-Sensitized Solar Cells. *RSC Adv.* **2013**, *3*, 559−565.

(12) Zhang, Q. F.; Myers, D.; Lan, J. L.; Jenekhe, S. A.; Cao, G. Z. Applications of Light Scattering in Dye-Sensitized Solar Cells. *Phys. Chem. Chem. Phys.* **2012**, *14*, 14982−14998.

(13) Li, L.-L.; Tsai, C.-Y.; Wu, H.-P.; Chen, C.-C.; Diau, E. W.-G. Fabrication of Long TiO_2 Nanotube Arrays in a Short Time Using a Hybrid Anodic Method for Highly Efficient Dye-Sensitized Solar Cells. *J. Mater. Chem.* **2010**, *20*, 2753−2758.

(14) Li, L.-L.; Chen, Y.-J.; Wu, H.-P.; Wang, N. S.; Diau, E. W.-G. Detachment and Transfer of Ordered TiO_2 Nanotube Arrays for Front-Illuminated Dye-Sensitized Solar Cells. *Energy Environ. Sci.* **2011**, *4*, 3420−3425.

(15) Zhou, Z. J.; Fan, J. Q.; Wang, X.; Zhou, W. H.; Du, Z. L.; Wu, S. X. Effect of Highly Ordered Single-Crystalline TiO_2 Nanowire Length on the Photovoltaic Performance of Dye-Sensitized Solar Cells. *ACS Appl. Mater. Interfaces* **2011**, *3*, 4349−4353.

(16) Feng, X.; Zhu, K.; Frank, A. J.; Grimes, C. A.; Mallouk, T. E. Rapid Charge Transport in Dye-Sensitized Solar Cells Made from Vertically Aligned Single-Crystal Rutile TiO_2 Nanowires. *Angew. Chem., Int. Ed.* **2012**, *51*, 2727−2730.

(17) Liao, J.-Y.; He, J.-W.; Xu, H.; Kuang, D.-B.; Su, C.-Y. Effect of TiO_2 Morphology on Photovoltaic Performance of Dye-Sensitized Solar Cells: Nanoparticles, Nanofibers, Hierarchical Spheres and Ellipsoid Spheres. *J. Mater. Chem.* **2012**, *22*, 7910−7918.

(18) Ghadiri, E.; Taghavinia, N.; Zakeeruddin, S. M.; Gratzel, M.; Moser, J. E. Enhanced Electron Collection Efficiency in Dye-Sensitized Solar Cells Based on Nanostructured TiO_2 Hollow Fibers. *Nano Lett.* **2010**, *10*, 1632−1638.

(19) Adachi, M.; Murata, Y.; Takao, J.; Jiu, J.; Sakamoto, M.; Wang, F. Highly Efficient Dye-Sensitized Solar Cells with a Titania Thin-Film Electrode Composed of a Network Structure of Single-Crystal-Like TiO_2 Nanowires Made by the "Oriented Attachment" Mechanism. *J. Am. Chem. Soc.* **2004**, *126*, 14943−14949.

(20) Jiu, J.; Isoda, S.; Wang, F.; Adachi, M. Dye-Sensitized Solar Cells Based on a Single-Crystalline TiO_2 Nanorod Film. *J. Phys. Chem. B* **2006**, *110*, 2087−2092.

(21) Kang, S. H.; Choi, S. H.; Kang, M. S.; Kim, J. Y.; Kim, H. S.; Hyeon, T.; Sung, Y. E. Nanorod-Based Dye-Sensitized Solar Cells with Improved Charge Collection Efficiency. *Adv. Mater.* **2008**, *20*, 54−58.

(22) Melcarne, G.; De Marco, L.; Carlino, E.; Martina, F.; Manca, M.; Cingolani, R.; Gigli, G.; Ciccarella, G. Surfactant-Free Synthesis of Pure Anatase TiO_2 Nanorods Suitable for Dye-Sensitized Solar Cells. *J. Mater. Chem.* **2010**, *20*, 7248−7254.

(23) Parmar, K. P.; Ramasamy, E.; Lee, J.; Lee, J. S. Rapid (Approximately 10 min) Synthesis of Single-Crystalline, Nanorice TiO_2 Mesoparticles with a High Photovoltaic Efficiency of above 8%. *Chem. Commun.* **2011**, *47*, 8572−8574.

(24) Kim, E. Y.; Lee, W. I.; Whang, C. M. Charge Transport Characteristics of Dye-Sensitized TiO_2 Nanorods with Different Aspect Ratios. *Bull. Korean Chem. Soc.* **2011**, *32*, 2671−2676.

(25) Buonsanti, R.; Carlino, E.; Giannini, C.; Altamura, D.; De Marco, L.; Giannuzzi, R.; Manca, M.; Gigli, G.; Cozzoli, P. D. Hyperbranched Anatase TiO_2 Nanocrystals: Nonaqueous Synthesis, Growth Mechanism, and Exploitation in Dye-Sensitized Solar Cells. *J. Am. Chem. Soc.* **2011**, *133*, 19216−19239.

(26) Rui, Y.; Li, Y.; Wang, H.; Zhang, Q. Photoanode Based on Chain-Shaped Anatase TiO_2 Nanorods for High-Efficiency Dye-Sensitized Solar Cells. *Chem. Asian J.* **2012**, *7*, 2313−2320.

(27) Tan, B.; Wu, Y. Dye-Sensitized Solar Cells Based on Anatase TiO_2 Nanoparticle/Nanowire Composites. *J. Phys. Chem. B* **2006**, *110*, 15932−15938.

(28) Chen, J.; Li, B.; Zheng, J.; Jia, S.; Zhao, J.; Jing, H.; Zhu, Z. Role of One-Dimensional Ribbonlike Nanostructures in Dye-Sensitized TiO_2-Based Solar Cells. *J. Phys. Chem. C* **2011**, *115*, 7104−7113.

(29) Wang, X. X.; Karanjit, S.; Zhang, L. F.; Fong, H.; Qiao, Q. Q.; Zhu, Z. T. Transient Photocurrent and Photovoltage Studies on Charge Transport in Dye Sensitized Solar Cells Made from the Composites of TiO_2 Nanofibers and Nanoparticles. *Appl. Phys. Lett.* **2011**, *98*, 082114-1−3.

(30) Mohammadpour, R.; Iraji zad, A.; Hagfeldt, A.; Boschloo, G. Investigation on the Dynamics of Electron Transport and Recombination in TiO_2 Nanotube/Nanoparticle Composite Electrodes for Dye-Sensitized Solar Cells. *Phys. Chem. Chem. Phys.* **2011**, *13*, 21487−21491.

(31) Sheng, J.; Hu, L.; Xu, S.; Liu, W.; Mo, L.; Tian, H.; Dai, S. Characteristics of Dye-Sensitized Solar Cells Based on the TiO_2

Nanotube/Nanoparticle Composite Electrodes. *J. Mater. Chem.* **2011**, *21*, 5457−5463.
(32) Lee, B. H.; Song, M. Y.; Jang, S.-Y.; Jo, S. M.; Kwak, S.-Y.; Kim, D. Y. Charge Transport Characteristics of High Efficiency Dye-Sensitized Solar Cells Based on Electrospun TiO_2 Nanorod Photoelectrodes. *J. Phys. Chem. C* **2009**, *113*, 21453−21457.
(33) Sauvage, F.; Di Fonzo, F.; Li Bassi, A.; Casari, C. S.; Russo, V.; Divitini, G.; Ducati, C.; Bottani, C. E.; Comte, P.; Grätzel, M. Hierarchical TiO_2 Photoanode for Dye-Sensitized Solar Cells. *Nano Lett.* **2010**, *10*, 2562−2567.
(34) Qu, J.; Li, G. R.; Gao, X. P. One-Dimensional Hierarchical Titania for Fast Reaction Kinetics of Photoanode Materials of Dye-Sensitized Solar Cells. *Energy Environ. Sci.* **2010**, *3*, 2003−2009.
(35) Zhuge, F.; Qiu, J.; Li, X.; Gao, X.; Gan, X.; Yu, W. Toward Hierarchical TiO_2 Nanotube Arrays for Efficient Dye-Sensitized Solar Cells. *Adv. Mater.* **2011**, *23*, 1330−1334.
(36) Yang, L.; Leung, W. W. Application of a Bilayer TiO_2 Nanofiber Photoanode for Optimization of Dye-Sensitized Solar Cells. *Adv. Mater.* **2011**, *23*, 4559−4562.
(37) Liao, J. Y.; Lei, B. X.; Kuang, D. B.; Su, C. Y. Tri-Functional Hierarchical TiO_2 Spheres Consisting of Anatase Nanorods and Nanoparticles for High Efficiency Dye-Sensitized Solar Cells. *Energy Environ. Sci.* **2011**, *4*, 4079−4085.
(38) Zhu, F.; Wu, D.; Li, Q.; Dong, H.; Li, J.; Jiang, K.; Xu, D. Hierarchical TiO_2 Microspheres: Synthesis, Structural Control and Their Applications in Dye-Sensitized Solar Cells. *RSC Adv.* **2012**, *2*, 11629−11637.
(39) Chen, D.; Caruso, R. A. Recent Progress in the Synthesis of Spherical Titania Nanostructures and Their Applications. *Adv. Funct. Mater.* **2013**, *23*, 1356−1374.
(40) Qiu, Y.; Chen, W.; Yang, S. Double-Layered Photoanodes from Variable-Size Anatase TiO_2 Nanospindles: a Candidate for High-Efficiency Dye-Sensitized Solar Cells. *Angew. Chem., Int. Ed.* **2010**, *122*, 3757−3761.
(41) Nazeeruddin, M. K.; De Angelis, F.; Fantacci, S.; Selloni, A.; Viscardi, G.; Liska, P.; Ito, S.; Takeru, B.; Gratzel, M. Combined Experimental and DFT-TDDFT Computational Study of Photoelectrochemical Cell Ruthenium Sensitizers. *J. Am. Chem. Soc.* **2005**, *127*, 16835−16847.
(42) Wang, Q.; Ito, S.; Gratzel, M.; Fabregat-Santiago, F.; Mora-Sero, I.; Bisquert, J.; Bessho, T.; Imai, H. Characteristics of High Efficiency Dye-Sensitized Solar Cells. *J. Phys. Chem. B* **2006**, *110*, 25210−25221.
(43) Wang, Z. S.; Kawauchi, H.; Kashima, T.; Arakawa, H. Significant Influence of TiO_2 Photoelectrode Morphology on the Energy Conversion Efficiency of N719 Dye-Sensitized Solar Cell. *Coordin. Chem. Rev.* **2004**, *248*, 1381−1389.
(44) Wang, P.; Zakeeruddin, S. M.; Comte, P.; Charvet, R.; Humphry-Baker, R.; Grätzel, M. Enhance the Performance of Dye-Sensitized Solar Cells by Co-grafting Amphiphilic Sensitizer and Hexadecylmalonic Acid on TiO_2 Nanocrystals. *J. Phys. Chem. B* **2003**, *107*, 14336−14341.
(45) Wang, P.; Zakeeruddin, S. M.; Moser, J. E.; Nazeeruddin, M. K.; Sekiguchi, T.; Grätzel, M. A Stable Quasi-Solid-State Dye-Sensitized Solar Cell with an Amphiphilic Ruthenium Sensitizer and Polymer Gel Electrolyte. *Nat. Mater.* **2003**, *2*, 402−407.
(46) Cao, Y.; Bai, Y.; Yu, Q.; Cheng, Y.; Liu, S.; Shi, D.; Gao, F.; Wang, P. Dye-Sensitized Solar Cells with a High Absorptivity Ruthenium Sensitizer Featuring a 2-(Hexylthio)thiophene Conjugated Bipyridine. *J. Phys. Chem. C* **2009**, *113*, 6290−6297.
(47) Yu, Q.; Liu, S.; Zhang, M.; Cai, N.; Wang, Y.; Wang, P. An Extremely High Molar Extinction Coefficient Ruthenium Sensitizer in Dye-Sensitized Solar Cells: The Effects of π-Conjugation Extension. *J. Phys. Chem. C* **2009**, *113*, 14559−14566.
(48) Ito, S.; Chen, P.; Comte, P.; Nazeeruddin, M. K.; Liska, P.; Péchy, P.; Grätzel, M. Fabrication of Screen-Printing Pastes from TiO_2 Powders for Dye-Sensitised Solar Cells. *Prog. Photovoltaics Res. Appl.* **2007**, *15*, 603−612.